

The Surface Laplacian Technique in EEG: Theory and Methods

Claudio Carvalhaes^{a,*}, J. Acacio de Barros^b

^a*Center for the Study of Language and Information, 220 Panama St, Stanford, CA
94305, USA*

^b*Liberal Studies, San Francisco State University, 1600 Holloway Ave, San Francisco, CA
94312*

Abstract

In this paper we review major theoretical and computational aspects of the surface Laplacian technique. Here we focus our attention on a few topics that are fundamental for a physical understanding of this technique and its efficient computational implementation. We highlight several issues that in our view deserve further research exploration, some of which we have attempted to address to the extent possible. We also included a set of approximations for the Laplacian on the border of a discrete grid and the description of an algorithm that accounts for the finite size of the measuring electrodes.

Keywords: surface Laplacian, high-resolution EEG, current source density

1. Introduction

The surface Laplacian technique is a powerful method to study EEG. It emerged back in the 1970's, from the seminal works of Nicholson (1973),

*Corresponding author

Email address: claudioc@stanford.edu (Claudio Carvalhaes)

Freeman and Nicholson (1975), Nicholson and Freeman (1975), and Hjorth (1975), and has ever since become increasingly popular. Hjorth's work was followed by efforts to develop better computational methods (see Gevins, 1988, 1989; Gevins et al., 1990; Perrin et al., 1989; Law et al., 1993a; Yao, 2002; Carvalhaes and Suppes, 2011) as well as attempts to combine the surface Laplacian with other methods (Kayser and Tenke, 2006a,b; Carvalhaes et al., 2009). Modern applications include studies on generators of event-related potentials (Kayser and Tenke, 2006a,b), spectral coherence (Srinivasan et al., 2007; Winter et al., 2007), event-related synchronization/desynchronization (Del Percio et al., 2007), phase-lock synchronization (Doesburg et al., 2008), estimation of cortical connectivity (Astolfi et al., 2007), high-frequency EEG (Fitzgibbon et al. (2013), just to mention a few.

The rationale of the surface Laplacian technique is grounded on Ohm's law, which establishes a local relationship between the surface Laplacian of scalp potentials and the underlying flow of electric current caused by brain activity (see Appendix in Carvalhaes et al., 2014). Presumably, this local relation should improve spatial resolution, reflecting electrical activity from a more restricted cortical area than what is observed in conventional topography.

In contrast to other high-resolution techniques, such as cortical surface imaging (Nunez et al., 1994; Yao, 1996; Yao et al., 2001), the surface Laplacian has the advantage of not requiring a volume conductor model of the head or a detailed specification of neural sources, but objections to it may

arise due to a combination of factors. First, there is a noticeable difficulty in understanding the technique in depth (Nunez and Westdorp, 1994). While EEG potentials can be physically understood in terms of current flow or in analogy with the gravitational potential, interpreting the surface Laplacian operation seems much less intuitive, as it involves the application of a second-order partial differential operator to a scalar potential distribution. Second, it appears surprising to many that one can actually obtain a reference-independent quantity from a signal which is seen to have been contaminated by a reference in its very origin (Nunez and Srinivasan, 2006, ch 7). Third, it is not possible to guarantee that the theoretical advantages associated to the use of the Laplacian differentiation will be preserved in the practical world of imperfect measurements and finite samples. In fact, reliable estimates of the Laplacian derivation are technically challenging, and computational methods to perform this task are still an intense subject of research.

The literature dedicated to provide theoretical explanations about the surface Laplacian technique is scarce, but it contains substantial and valuable information (see Nunez and Srinivasan, 2006; Tenke and Kayser, 2012). Nevertheless, there are still some gaps that, if filled, can help comprehension and permit a more intuitive view of the technique. It is the primary intention of this paper to contribute to this matter. For this purpose, Section 2 provides physical insights on the surface Laplacian technique that are often not discussed in the literature, but that are at the heart of some of the issues

of interest to the EEG researcher. Section 3 focuses on the computational aspects of this technique, providing a comprehensive review of selected computational methods and their limitations. In our view, some computation issues still need to be settled, for which we devoted two sections of this paper. In Section 3.5 we present a formulation of surface Laplacian estimates in terms of the transformation matrix, which is a data-independent structure for transforming raw signals into surface Laplacian derivations. Section 3.6 is devoted to discuss the regularization problem of smoothing splines that significantly affects surface Laplacian estimates. Finally, in the Concluding Remarks, we outline a procedure that incorporates the electrode size on the smoothing spline function to reflect the average nature of scalp-recorded EEG signals.

2. An Overview of the Physics of EEG

In this Section we discuss the main theoretical ideas behind the use of the surface Laplacian. Our goal here is to introduce some concepts from the physics of EEG that are often unfamiliar to the EEG researcher, and that have direct relevance to the the surface Laplacian technique. We do not attempt to reproduce the main arguments about the relationship between the surface Laplacian and the dura-surface potential, nor with the Current Source Density (CSD), which are found, for example, in Nunez and Srinivasan (2006) and Tenke and Kayser (2012). Instead we focus on the more fundamental aspects that are often overlooked.

2.1. Physical interpretation of the surface Laplacian

To better understand the physical meaning of the surface Laplacian operation, it is instructive to start with the volume Laplacian, or simply Laplacian, and its relationship to the quasi-static electric field and potential. Here our treatment is very standard, and can be found in more details in any textbook on electricity and magnetism, such as Jackson (1999) or Schey (2004), and the reader interested in more detail is referred to them. Our discussion will focus only on aspects that are directly relevant to EEG.

When we talk about scalp EEG, we are always referring to the potential with respect to some reference electrode. But, from a physics point of view, the *electric field* is more fundamental than the potential. To see this, let us recall that the field has a measurable effect: for a particle of charge q , the field $\mathbf{E}(\mathbf{r})$ at the position \mathbf{r} is operationally *defined* by the ratio between the electric force \mathbf{F}_E acting on the charge at \mathbf{r} and the value of q . Here we use the standard notation of representing scalar quantities in italics and vectors in boldface, e.g. q for the electric charge and \mathbf{E} for the electric field, and we also use the symbol “ \equiv ” for an equality that arises from a definition. From this definition, the field is a quantity that measures the force per unit of charge, i.e., \mathbf{E} (as a function of the position \mathbf{r}) is given by

$$\mathbf{E}(\mathbf{r}) \equiv \frac{1}{q} \mathbf{F}_E(\mathbf{r}). \quad (1)$$

For simplicity, we are ignoring any temporal dependence of \mathbf{E} , but the results

remains the same, for all practical purposes, in the typical range of frequencies involved in the brain electrical activity (Jackson, 1999; Nunez and Srinivasan, 2006).

Electric fields generated by point charges are described by Coulomb's Law. A consequence of this law is that \mathbf{E} is a conservative field, i.e., the line integral

$$V_{AB} = - \int_{\mathbf{r}_A}^{\mathbf{r}_B} \mathbf{E}(\mathbf{r}) \cdot d\mathbf{r} \quad (2)$$

between two points \mathbf{r}_A and \mathbf{r}_B is independent of the path along which it is computed. The value V_{AB} has an important physical meaning: it corresponds to the work per unit of charge necessary to be done on a charged particle when it goes through the field \mathbf{E} from position \mathbf{r}_A to \mathbf{r}_B at a constant speed. Thus, the quantity V_{AB} is not only measurable, but of practical use, as we will see later on. But also of importance is the fact that the path-independence of V_{AB} implies the existence of a function $V(\mathbf{r})$ such that

$$V_{AB} \equiv V(\mathbf{r}_B) - V(\mathbf{r}_A). \quad (3)$$

The function $V(\mathbf{r})$ is called the *electric potential* of the field \mathbf{E} .

One important relationship between the electric field \mathbf{E} and the potential V is given by the gradient operator. The gradient of $V(\mathbf{r})$, denoted $\text{Grad}(V(\mathbf{r}))$, is defined, in Cartesian coordinates, as

$$\text{Grad}(V(\mathbf{r})) = \frac{\partial V(\mathbf{r})}{\partial x} \hat{\mathbf{i}} + \frac{\partial V(\mathbf{r})}{\partial y} \hat{\mathbf{j}} + \frac{\partial V(\mathbf{r})}{\partial z} \hat{\mathbf{k}}, \quad (4)$$

where $\hat{\mathbf{i}}$, $\hat{\mathbf{j}}$, and $\hat{\mathbf{k}}$ are the orthonormal basis vectors. The gradient forms a vector field such that, at point \mathbf{r}' , it has the following properties. For a unitary vector $\hat{\mathbf{u}}$, $\text{Grad}(V(\mathbf{r}')) \cdot \hat{\mathbf{u}}$ gives the rate of change of the function $V(\mathbf{r})$ in the direction $\hat{\mathbf{u}}$, and $\text{Grad}(V(\mathbf{r}'))$ at point \mathbf{r}' is a vector pointing at the direction where the function V changes the most. In other words, the direction perpendicular to $\text{Grad}(V(\mathbf{r}'))$ points at the direction of the *isopotential lines*. From this, it is possible to prove that the function $V(\mathbf{r})$ relates to the field by the expression

$$\mathbf{E}(\mathbf{r}) = -\text{Grad}(V(\mathbf{r})), \quad (5)$$

i.e., the electric field is the negative gradient of the electric potential.

It is easy to see that $V(\mathbf{r})$ is not uniquely defined, as any other function $V'(\mathbf{r})$ given by

$$V'(\mathbf{r}) \equiv V(\mathbf{r}) - V_0, \quad (6)$$

where V_0 is an arbitrary constant, also gives the same differences of potential V_{AB} between positions \mathbf{r}_A and \mathbf{r}_B , and therefore the same gradient (for instance, when we take the limit of $\Delta\mathbf{r} = \mathbf{r}_B - \mathbf{r}_A$ very small). As an example, let us consider the electric field from a point particle with charge q situated at position \mathbf{r}_0 , which is given by

$$\mathbf{E}(\mathbf{r}) = \frac{q}{4\pi\epsilon_0} \frac{\mathbf{r} - \mathbf{r}_0}{(\mathbf{r} - \mathbf{r}_0)^3}.$$

It is easy to show that a potential function satisfying (2) is given by

$$V(\mathbf{r}) = -\frac{q}{4\pi\epsilon_0} \frac{1}{|\mathbf{r} - \mathbf{r}_0|}. \quad (7)$$

For another potential function V' given by $V'(\mathbf{r}) = -\frac{q}{4\pi\epsilon_0} \frac{1}{|\mathbf{r} - \mathbf{r}_0|} + V_0$, we see at once that its gradient is exactly the same as for $V(\mathbf{r})$, since any constant added to V would disappear when the derivative in (4) is taken. However, the potential (7) is often given in textbooks, as it has the feature that the potential is zero in infinity ($V \rightarrow 0$ when $|\mathbf{r}| \rightarrow \infty$), which corresponds to a reference in a point infinitely distant from \mathbf{r}_0 .

As we mentioned above, the potential difference has practical use. This is because in a conductor with non-zero electrical resistance an electric field produces a current density \mathbf{j} given by

$$\mathbf{E}(\mathbf{r}) = \rho \mathbf{j}(\mathbf{r}), \quad (8)$$

$\rho = 1/\sigma$ is the resistivity, given by the inverse of the conductivity σ . Equation (8) is sometimes referred to as the vector form of Ohm's Law, for the following reason. For practical measurements, directly observing the electric field is very difficult, but measuring the current flow between two points \mathbf{r}_A and \mathbf{r}_B is not. Given (8), it follows, taking the integral on both sides, that this current flow is proportional to the potential difference $V(\mathbf{r}_B) - V(\mathbf{r}_A)$. Thus, in a conductive media with resistivity ρ , current measurements between different points can be used to construct a map of the potential function (minus a

reference value V_0 , which is often arbitrarily chosen such that $V(\mathbf{r}_{\mathcal{O}}) = 0$ at some reference point \mathcal{O}), which may be used to compute the electric field $\mathbf{E}(\mathbf{r})$. Here we must emphasize that electric potentials can *never* be directly measured; only potential differences between two points can.

Though in this paper we are interested in the surface Laplacian, for completeness we should also mention the physical meaning of the Laplacian. Such meaning comes from Gauss's Law, which in its differential form given by Maxwell is written as

$$\text{Div}(\mathbf{E}) = 4\pi\rho_Q, \quad (9)$$

where ρ_Q is the charge density¹. This law has the immediate physical interpretation that electric charges are sources of an electric field: if there are no electric charges, the divergence of the field is zero. Now, from equation (5) we have at once that, from (5),

$$\text{Div}(\mathbf{E}) = -\text{Div}(\text{Grad}(V)). \quad (10)$$

The divergence of the gradient, $\text{Div}(\text{Grad}(V))$, is defined as the Laplacian of V , denoted by $\text{Lap}(V) \equiv \text{Div}(\text{Grad}(V))$. Thus, from (10) and (9) it follows that the Laplacian of the potential is proportional to the electric field sources, i.e.,

$$\text{Lap}(V) = -4\pi\rho_Q. \quad (11)$$

¹Usually in physics the charge density is represented by ρ , but here we use the subscript Q to distinguish it from the resistivity, defined as $\rho = 1/\sigma$.

The above discussion was intended to show the connection between the field \mathbf{E} to the scalar potential V . However, in its generality, it does not take into account some specific characteristics of the EEG. First, the EEG is measured over the scalp, which is geometrically a curved surface. Second, such measurements are not directly of the field, but are instead differences of potential associated to small current flows between two electrodes (often between a measuring and a reference electrode). Finally, because such measurements are on the scalp, they happen where there is a significant change in conductivity (interface scalp/air). All of those points have some consequence for the interpretations of the field and Laplacian.

Starting with the Laplacian, the most common assumption is that sources of interest to the EEG are inside the skull, and that there are no sources on the scalp itself (Nunez and Srinivasan, 2006). This, of course, is an approximation, given that even EEG electrodes can chemically generate currents. But if we start with this assumption, we have that, from (9),

$$\text{Lap}(V) = 0. \tag{12}$$

Using the expression for the Laplacian in Cartesian coordinates, we have

$$\frac{\partial^2 V}{\partial x^2} + \frac{\partial^2 V}{\partial y^2} + \frac{\partial^2 V}{\partial z^2} = 0. \tag{13}$$

Let us now choose the coordinate system such that the scalp is on the plane x, y (for small areas, this is a good approximation). Then we can rewrite

(13) as

$$\frac{\partial^2 V}{\partial x^2} + \frac{\partial^2 V}{\partial y^2} = \frac{\partial E}{\partial z}, \quad (14)$$

where on the right hand side we used the relationship between the field and the potential. Remembering that in a conductor $\mathbf{E} = \rho \mathbf{j}$, it follows that

$$\frac{\partial^2 V}{\partial x^2} + \frac{\partial^2 V}{\partial y^2} = \rho \frac{\partial j_z}{\partial z}. \quad (15)$$

The left hand side of (15) is defined as the *surface Laplacian* of V ,

$$\text{Lap}_S(V) = \frac{\partial^2 V}{\partial x^2} + \frac{\partial^2 V}{\partial y^2}, \quad (16)$$

and (15) shows that $\text{Lap}_S(V)$ is related to *how fast the normal component of the current changes in the direction perpendicular to the surface*. Thus, if $\text{Lap}_S(V)$ is nonzero, conceptually, in the absence of sources, the current change in this direction means a fanning out of the current lines, i.e., a spreading out of the currents. In the case of the scalp, this means that a nonzero $\text{Lap}_S(V)$ corresponds to *diverging* (with respect to the radial direction) *current lines under the scalp*, which is associated to the presence of a source of currents inside the skull. Thus, we see that the surface Laplacian has a direct relationship to currents under the scalp, and it can be shown that it is related to electrical activities on the dura surface (Nunez and Srinivasan, 2006).

2.2. Properties of the surface Laplacian

Equipped with an interpretation of the surface Laplacian in terms of currents and fields, we now turn to some of its important properties. Let us start with one of the main characteristics of the surface Laplacian: it is *reference free*. This may seem puzzling to some, as in most cases the surface Laplacian is computed from the scalp potential, which is itself a reference-dependent quantity. To understand how this is possible, it is worth examining a simple example from geometry. Imagine we have two points, P and Q , representing the locations of two events of interest. From an observer using the coordinate system \mathcal{O} (see Figure 1), the positions of P and Q are given by the (reference-dependent) vectors \mathbf{r}_P and \mathbf{r}_Q . That the position vectors of P and Q are reference dependent can be seen by the simple fact that another observer using coordinates \mathcal{O}' describe such positions by the vectors \mathbf{r}'_P and \mathbf{r}'_Q , which are clearly different from \mathbf{r}_P and \mathbf{r}_Q . Thus, the geometrical meaning of, say, the length of the position vector \mathbf{r}_P , is not related to the event of interest only, but to a combination of such event and an *arbitrary* choice of reference system, making this quantity reference dependent.

However, there are many geometrically reference-free quantities, i.e., quantities that look the same for \mathcal{O} and \mathcal{O}' , that can be constructed from the reference-dependent positions \mathbf{r}_P and \mathbf{r}_Q . For example, the vector connecting P and Q is reference-free, since it is given by $\mathbf{r} = \mathbf{r}_P - \mathbf{r}_Q = \mathbf{r}'_P - \mathbf{r}'_Q$. Notice that \mathbf{r} has the feature of depending only on characteristics of the system of interest, P and Q . Another important reference-free quantity is

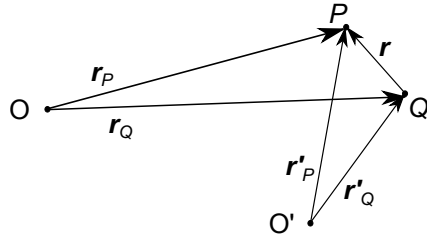


Figure 1: Events P and Q as observed from \mathcal{O} and \mathcal{O}' .

the distance d between P and Q , defined by $d^2 = \mathbf{r}^2 = (\mathbf{r}_P - \mathbf{r}_Q) \cdot (\mathbf{r}_P - \mathbf{r}_Q)$. Thus, from reference-dependent geometrical quantities it is possible to obtain reference-free ones.

For the EEG, the reference-free property is not unrelated to the fact that the surface Laplacian has physical meaning, whereas the scalp potential does not. For instance, as we saw above, the electric field is operationally defined by its effect on a test charge. In a medium where the electric resistance σ is non-zero, such as in the brain, skull, or scalp, this effect translates into a (local) current given by

$$\mathbf{E} = \rho \mathbf{j}, \quad (17)$$

where $\rho = 1/\sigma$ is the resistivity and \mathbf{j} is the electric current density. The electric potential, on the other hand, is not operationally defined; instead, the *difference* of potential between two points is. For instance, as we saw above, in most EEG experiments what is measured is actually the current flowing between two electrodes, which is proportional to the difference of potential between the two electrode positions. So, if we define a potential function $V(\mathbf{r})$, the value of such function tells us nothing about measurable

quantities in \mathbf{r} ; what is measurable is the potential difference between two observation points, $\Delta V = V(\mathbf{r}') - V(\mathbf{r})$. In other words, from a physical point of view it makes no sense to say that the potential at a point P is, for instance, $V(\mathbf{r}_P)$; however, it does make sense to say that the electric field at point P is $\mathbf{E}(\mathbf{r}_P)$. From the electric field we can obtain the Laplacian, given by $\text{Div}(\mathbf{E})$. Thus, the Laplacian is simply the divergence of \mathbf{E} , and as such is nonzero where there are sinks or sources of electric field.

In practice, directly measuring the scalp field or surface Laplacian is technically very difficult. However, measuring differences of potential between two points on the scalp is technically easy. Because of this, it is common, as we mentioned above, to use the observed differences of potential (often defined against a reference electrode) to calculate the surface Laplacian or the electric field (see Section 3 for computational methods).

Of course, being reference free does not mean that the surface Laplacian of V computed from an EEG is not subject to problems due to a bad choice of reference electrodes. To understand this, let us imagine that we have two nearby points of interest on the scalp, say P_1 and P_2 . Their electric potential difference $\Delta V_{12} = V(\mathbf{r}_2) - V(\mathbf{r}_1)$, where \mathbf{r}_1 and \mathbf{r}_2 are the positions of P_1 and P_2 , is physically relevant (and reference free), since it is proportional to the work done by the electric field on a test charge moving from P_1 to P_2 . This potential difference can be observed either by measuring the current flow between P_1 and P_2 , which is proportional to ΔV_{12} , or by measuring the current flow between each point P_1 and P_2 with respect to another point

R , the place of a reference electrode. Since $\Delta V_{1R} = V(\mathbf{r}_1) - V(\mathbf{r}_R)$ and $\Delta V_{2R} = V(\mathbf{r}_2) - V(\mathbf{r}_R)$, it follows that

$$\Delta V_{12} = \Delta V_{2R} - \Delta V_{1R}. \quad (18)$$

As we will see below in Section 3, both the electric field and the Laplacian may be computed from terms such as $\Delta V_{2R} - \Delta V_{1R}$. But expressions like equation (18) overlook an important problem: recording and data acquisition conditions. For instance, the choice of a reference electrode that is too far away (say, on the left foot) will cause a reduction on the measured current between, say, P_1 and R ; such a decreased current will translate into a lower signal-to-noise ratio. Because of the presence of random noise, $\Delta V_{2R} - \Delta V_{1R}$ is not exactly the same as ΔV_{12} (neither is the actual bipolar measurement), but a bad choice of electrode makes this problem even more pronounced.

The above discussion holds for the general case, being valid for all cases where a quasi-static electric field interaction is involved (Hämäläinen et al., 1993). We included such discussion here because it is seldom present in the EEG review literature, but it bears relevance to many of the concepts often overlooked. We now turn to a description of the computational methods.

3. Computational Methods

We recall from Section 2.1 that the surface Laplacian is a mathematical operation that involves a combination of partial derivatives. In practice,

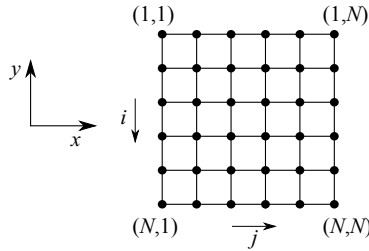


Figure 2: Coordinate system of the continuous variables x and y and the mapping into grid nodes in terms of the discrete variables i and j .

however, we need to operate on the basis of a discrete signal. Numerical procedures for this computation fall generally into two main categories, *finite difference* and *mesh-free methods*. Our goal in this Section is to review methods of both types and emphasize issues related to each.

3.1. Finite difference methods

Generally speaking, finite difference methods consist of a *discretization procedure* for differential operations in which a continuous domain is transformed into a mesh of discrete points. For surface Laplacian estimates, two major assumptions are commonly made to simplify calculations and arrive at a quite useful approximation. First, the scalp surface is taken as locally flat, leading to the following differential form in Cartesian coordinates (see also Section 2.1)

$$\text{Lap}_s(V) = \frac{\partial^2 V}{\partial x^2} + \frac{\partial^2 V}{\partial y^2}. \quad (19)$$

Second, the measuring electrodes are assumed to be equidistant (this is hardly the case), forming a square grid of size h , each electrode occupying an individual node of the grid, as shown in Figure 2. With these considerations,

a finite difference approximation for the surface Laplacian of V at a grid node (i, j) is given by (Abramowitz and Stegun, 1964, 25.3.30)

$$\text{Lap}_s(V)|_{(i,j)} \approx \frac{V_{(i-1,j)} + V_{(i+1,j)} + V_{(i,j-1)} + V_{(i,j+1)} - 4V_{(i,j)}}{h^2}. \quad (20)$$

The mathematics behind this approximation is nontrivial, and for completeness we present a detailed explanation in the Appendix.

The right hand side of (20) can be interpreted as a mathematical change in reference for the potential $V_{(i,j)}$ to the average over the four nearest neighbors. Due to the number of nodes composing this approximation, it is often referred to as a *5-point approximation*. The multiplicative factor $1/h^2$ ensures the correct physical unit for $\text{Lap}_s(V)$, but usually it can be taken as 1 (or any other constant) to facilitate calculations, as originally done in Hjorth (1975).

As we should expect from the discussion of Section 2.2, this approximation is reference-free: just replace V with $V' - V_{\text{ref}}$ at each node and note that the common reference signal V_{ref} is canceled. Assuming that the reference electrode lies at a central node, we can easily reconstruct $\text{Lap}_s(V)$ at the reference site, obtaining

$$\text{Lap}_s(V_{\text{ref}}) \approx \frac{V_{(i-1,j)} + V_{(i+1,j)} + V_{(i,j-1)} + V_{(i,j+1)}}{h^2}. \quad (21)$$

In the context of EEG, the expression (20) is normally referred to as

*Hjorth's approximation*². A limitation of this approximation is that it applies only to electrodes that are located at a central node, not accounting for estimates along the border of the grid. For border electrodes, Hjorth suggested a less accurate approximation that uses two-nearest neighbors along the border. An improvement on this scheme is to include other two electrodes to account for variations of V perpendicular to the border, which we have developed in the Appendix. For instance, for an electrode located along the left border, where $j = 1$, we have

$$\text{Lap}_s(V_{(i,1)}) \approx \frac{V_{(i-1,1)} + V_{(i+1,1)} - 2V_{(i,2)} + V_{(i,3)} - V_{(i,1)}}{h^2}, \quad (22)$$

and at the upper-left corner $(1, 1)$

$$\text{Lap}_s(V_{(1,1)}) \approx \frac{-2V_{(1,2)} + V_{(1,3)} - 2V_{(2,1)} + V_{(3,1)} + 2V_{(1,1)}}{h^2}. \quad (23)$$

As it occurs with the approximation (20), the nodes have weights that sum to zero, canceling electrical activity from the reference site in both approximations.

The geometric arrangements of electrodes in the above approximations are called *five-point stencils* and are illustrated in Figure 3. It is possible to construct approximations with more than five points following the same pro-

²We also acknowledge the work of Freeman and Nicholson (1975), who employed a discretization scheme to approximate the Laplacian of extra-cellular potentials in CSD analysis.

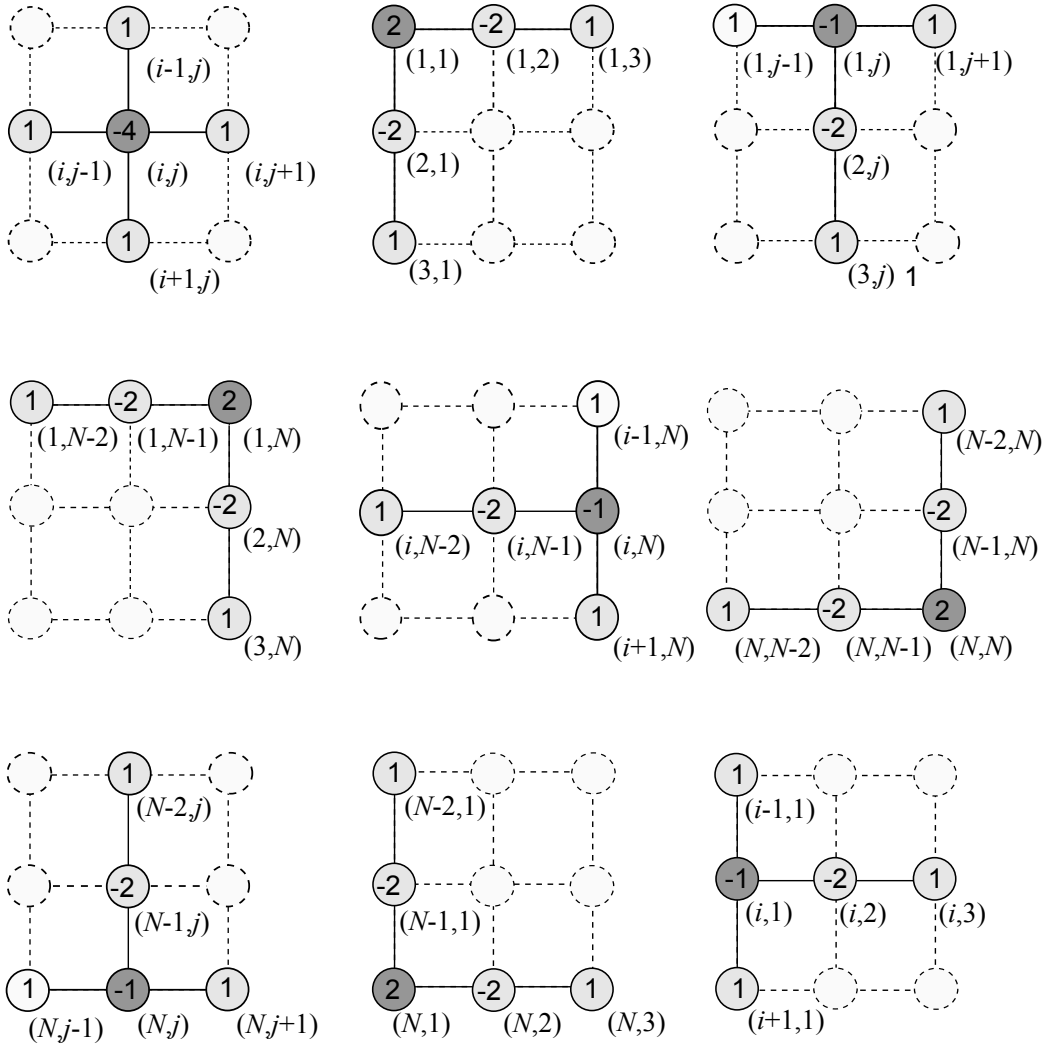


Figure 3: Five-point stencils to approximate $\text{Lap}_s(V)$ in a discrete grid.

cedure developed in the Appendix. But for several reasons a more complex approximation will not translate necessarily into more accurate results, and it is likely that the choice for five-point stencils is sufficient. Approximations using unevenly distributed electrodes can also be derived, but we will not address this in this paper (cf. Tenke et al., 1998).

Finite difference provides us with a simple measure of accuracy in terms of powers of the discretization parameter h . As explained in the Appendix, this measure is related to error due to the truncation of an infinite series to derive the approximation. For instance, approximation (20) is said to be accurate to the second-order of h , shorthand $\mathcal{O}(h^2)$, while for peripheral electrodes the five-point approximations (22) and (23) are accurate to $\mathcal{O}(h)$. In principle, making h small by using a high-density electrode array reduces truncation error and produces more accurate results. A small h is useful also to reduce error due to the unrealistic geometry of the planar scalp model, which is more prominent when averaging over sparse electrode sites. In the absence of an appropriate mechanism for regulation, high-density arrays can help reduce influence of non-local activities from unrelated sources.

But exceptions are expected to occur, as all this reasoning was based on the assumption of a point electrode, which ignores boundary effects produced by an actual electrode of finite size. Perhaps for this reason, and due to factors that we are not able to point out, McFarland et al. (1997) reported better estimates using next-nearest-neighbor approximations in comparison to nearest-neighbor approximations. Similar conclusion was drawn

by Müller-Gerking et al. (1999) in the context of EEG classification. In fact, next-nearest neighbor approximations have been adopted in CSD analysis since Freeman and Nicholson (1975) as a way to reduce high-frequency noise in the vicinity of an electrode. The trade-off between noise attenuation and loss of spatial resolution in low-density arrays was discussed by Tenke et al. (1993). In fact, lower-density estimates has proven to be quite useful more than once, as described by Kayser and Tenke (2006b) in the context of ERP analysis. Finally, we point out that evidence for electrode bridges in high-density EEG recordings has been identified as a problem, caused typically by electrolyte spreading between nearby electrodes (Tenke and Kayser, 2001; Greischar et al., 2004; Alschuler et al., 2014).

An efficient way to implement the above approximations and subsequent ones is via a *transformation matrix*, which will be discussed in Section 3.5

3.2. Smoothing thin-plate Laplacians

As an alternative to finite difference, *mesh-free* (or *grid-free*) methods allow for a much more flexible configuration of electrodes and are not restricted to a planar scalp mode. The Laplacian operation is performed analytically on a continuous function built directly from the data, without need for discretization. This function is obtained through interpolation or data smoothing. In the context of interpolation, the problem to be solved can be formulated as follows: given a set of measurements, say a potential distribution V_1, \dots, V_N , recorded from locations $\mathbf{r}_1, \dots, \mathbf{r}_N$, find a real function $f(\mathbf{r})$

such that $f(\mathbf{r}_i) = V_i$ for $i = 1, \dots, N$. This constraint is replaced with the condition that $f(\mathbf{r}_i)$ fits the data closely, but not exactly, in data smoothing, which serve to reduce variance due to noise. The method of *thin-plate spline* discussed here is a prime tool in both cases.

In three-dimensional Euclidean space the spline function is defined by (Wahba, 1990; Wood, 2003)

$$f(\mathbf{r}) = \sum_{i=1}^N c_i |\mathbf{r} - \mathbf{r}_i|^{2m-3} + \sum_{\ell=1}^M d_\ell \nu_\ell(\mathbf{r}), \quad (m \geq 2), \quad (24)$$

where m is an integer parameter, $M = \binom{m+2}{3}$ is subject to $M < N$, and ν_1, \dots, ν_M are linearly independent polynomials in three variables of degree less than m . The surface Laplacian differentiation of $f(\mathbf{r})$ requires that $m \geq 3$. The reader is referred to Carvalhaes and Suppes (2011) for the details of how to generate the polynomials ν_1, \dots, ν_M and determine the unknowns c_i 's and d_i 's. An important results is that, provided that $\mathbf{r}_1 \neq \mathbf{r}_2 \neq \dots \neq \mathbf{r}_N$, the function (24) is the unique minimizer of (Duchon, 1977; Meinguet, 1979; Wahba, 1990; Hastie et al., 2009, p.140)

$$\text{RSS}(f, \lambda) = \frac{1}{N} \sum_i (V_i - f(\mathbf{r}_i))^2 + \lambda J_m[f]. \quad (25)$$

The term $J_m[f]$ is a measure of roughness of the spline function in terms of its m -th-order partial derivatives, such that $J_m[\nu_\ell] = 0$ (Wahba, 1990). The parameter λ is *tuning parameter* that trades off between goodness of fit ($\lambda = 0$) and smoothness ($\lambda > 0$).

Using matrix notation, the unknowns c_i 's and d_i 's are determined by the linear system (Duchon, 1977; Meinguet, 1979; Wahba, 1990; Green and Silverman, 1994; Eubank, 1999)

$$\begin{pmatrix} \mathbf{K} + N\lambda\mathbf{I} & \mathbf{T} \\ \mathbf{T}^T & \mathbf{0} \end{pmatrix} \begin{pmatrix} \mathbf{c} \\ \mathbf{d} \end{pmatrix} = \begin{pmatrix} \mathbf{v} \\ \mathbf{0} \end{pmatrix}, \quad (26)$$

where $\mathbf{c} = (c_1, \dots, c_N)^T$, $\mathbf{d} = (d_1, \dots, d_M)^T$, $(\mathbf{K})_{ij} = |\mathbf{r}_j - \mathbf{r}_i|^{2m-3}$, $(\mathbf{T})_{ij} = \nu_j(\mathbf{r}_i)$, and $\mathbf{v} = (V_1, \dots, V_N)^T$ is the given potential distribution. The superscript T indicates transpose operation and \mathbf{I} is the $N \times N$ identity matrix. This system has the formal solution (Wahba, 1990)

$$\mathbf{c} = \mathbf{Q}_2 [\mathbf{Q}_2^T (\mathbf{K} + N\lambda\mathbf{I}) \mathbf{Q}_2]^{-1} \mathbf{Q}_2^T \mathbf{v}, \quad (27a)$$

$$\mathbf{R}\mathbf{d} = \mathbf{Q}_1^T (\mathbf{v} - \mathbf{K}\mathbf{c} - N\lambda\mathbf{c}), \quad (27b)$$

where $\mathbf{Q}_1 \in \mathbb{R}^{N \times N}$, $\mathbf{Q}_2 \in \mathbb{R}^{N \times (N-M)}$, and $\mathbf{R} \in \mathbb{R}^{N \times M}$ derive from the *QR-factorization* of \mathbf{T} ³:

$$\mathbf{T} = [\mathbf{Q}_1 \mid \mathbf{Q}_2] \begin{pmatrix} \mathbf{R} \\ \mathbf{0} \end{pmatrix}. \quad (28)$$

This approach has a major deficiency: it does not apply to data on a spherical or an ellipsoidal surface. To understand this limitation, consider the case

³The Matlab command for the QR-factorization of T is `[Q,R]=qr(T)`.

$m = 3$, for which the matrix \mathbf{T} can be expressed as

$$\mathbf{T} = \begin{pmatrix} 1 & x_1 & y_1 & z_1 & x_1^2 & x_1 y_1 & x_1 z_1 & y_1^2 & y_1 z_1 & z_1^2 \\ \vdots & \vdots & \vdots & \vdots & \vdots & \vdots & \vdots & \vdots & \vdots & \vdots \\ 1 & x_N & y_N & z_N & x_N^2 & x_N y_N & x_N z_N & y_N^2 & y_N z_N & z_N^2 \end{pmatrix}. \quad (29)$$

Since spherical and ellipsoidal surfaces are described by

$$\frac{x^2}{a^2} + \frac{y^2}{b^2} + \frac{z^2}{c^2} = 1, \quad a, b, c > 0, \quad (30)$$

where $a = b = c$ for a sphere, the 1st, 5th, 8th, and 10th columns of \mathbf{T} are *linearly dependent*, i.e., a combination of these columns with weights -1 , $1/a^2$, $1/b^2$ and $1/c^2$ yields zero. Therefore, \mathbf{T} has 10 columns but only 9 of them are linearly independent. This makes the linear system (26) *singular*, so that the unknowns c_i 's and d_i 's cannot be uniquely determined.

The singularity of (26) on spheres and ellipsoids affects only the transformation parametrized by \mathbf{d} , leaving intact the transformation specified by \mathbf{c} . It is therefore natural to try a minimum norm solution to this problem by determining \mathbf{d} using the *pseudo-inverse* of \mathbf{R} , i.e., $\mathbf{d} = \mathbf{R}^+ \mathbf{Q}'_1 (\mathbf{v} - \mathbf{Kc} - N\lambda\mathbf{c})$. This approach was proposed by Carvalhaes and Suppes (2011) (see also Carvalhaes (2013)), who evaluated its performance in the localization of cortical activity using spherical and ellipsoidal scalp models. Simulations using over 30,000 configurations of radial dipoles resulted in a success rate above 94.5% for the correct localization of cortical source at the closest electrode. This result

improved to 99.5% when the goal was simply to locate the source at one of the two closest electrode. Prediction error occurred more often for sources generating very small or very large peaks of amplitude, but it decreased substantially with increasing the number of electrodes in the simulation. In a study using empirical data the surface Laplacian of (24) outperformed finite difference and the method of spherical splines (see below) for all participants. The expressions for the surface Laplacian of the potential on spherical and ellipsoidal scalp models are provided in Carvalhaes and Suppes (2011), along with a Matlab implementation.

Similar to finite difference, spline estimates (as well as estimates with the methods discussed below) also are affected by the density of the electrode array, with high-density arrays resulting in more accurate estimates. However, some preparation issues such as electrolyte bridges are mainly a characteristic of high-density estimates and should be a concern, as it is for finite difference. From a numerical analysis standpoint, increasing the number of electrodes has the additional problem of making the system (26) increasingly sensitive to error (noise) in the input vector \mathbf{v} . Nevertheless, according to results in Sibson and Stone (1991) it is expected that montages with up to 256 electrodes result in reliable estimates using double-precision calculations.

Section 3.5 outlines the computational implementation of spline estimates through linear transformation. The tuning parameter λ determines the ability of the smoothing spline function (24) to compensate for spatial noise and is critical for a good performance of the estimate. The method of *general-*

ized cross validation presented in Section 3.6 provides a reasonable means for choosing this parameter.

3.3. Smoothing spherical splines

For the particular case of data points on spheres, Wahba developed a pseudo-spline method that circumvent the singularity of (26) by replacing the Euclidean distance with the geodesic distance. This method, called *spherical splines*, was used by Perrin et al. (1989) to developed one of the most popular surface Laplacian methods in the literature. The spherical interpolating function is defined as

$$f_{sph}(\mathbf{r}) = \sum_{i=1}^N c_i g_m(\mathbf{r}, \mathbf{r}_i) + d, \quad (31a)$$

where

$$g_m(\mathbf{r}, \mathbf{r}_i) = \frac{1}{4\pi} \sum_{\ell=1}^{\infty} \frac{2\ell + 1}{\ell^m (\ell + 1)^m} P_{\ell}(\hat{\mathbf{r}} \cdot \hat{\mathbf{r}}_i). \quad (31b)$$

The vectors \mathbf{r} and \mathbf{r}_i 's have length equal to the head radius and carets denote unit vectors, i.e., $\hat{\mathbf{r}} = \mathbf{r}/r$ and $\hat{\mathbf{r}}_i = \mathbf{r}_i/r$, so that the scalar product $\hat{\mathbf{r}} \cdot \hat{\mathbf{r}}_i$ gives the cosine of the angle between \mathbf{r} and \mathbf{r}_i . The parameter m is an integer larger than 1 and the one-variable functions P_{ℓ} 's are Legendre polynomials of degree ℓ . These polynomials occur in many problems in mathematical physics and their properties are listed in Abramowitz and Stegun (1964). The parameters c_1, \dots, c_N and d are determined by (27).

To apply the surface Laplacian to (31) we use spherical coordinates. Our

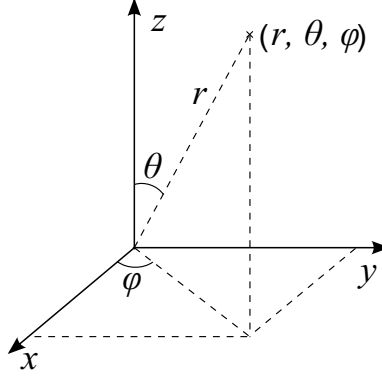


Figure 4: Spherical coordinate system.

convention is that of Figure 4: the polar angle $\theta \in [0, \pi]$ is measured down from the vertex, and the azimuthal angle $\varphi \in [0, 2\pi]$ increases counterclockwise from the x axis, which is directed towards the nasion. With this convention,

$$\text{Lap}_s(f) = \frac{1}{r^2 \sin \theta} \frac{\partial}{\partial \theta} \left[\sin \theta \frac{\partial f}{\partial \theta} \right] + \frac{1}{r^2 \sin^2 \theta} \frac{\partial^2 f}{\partial \varphi^2}. \quad (32)$$

It can be proved that the Legendre polynomials satisfy (Jackson, 1999, p. 110)

$$\text{Lap}_s(P_\ell(\hat{\mathbf{r}} \cdot \hat{\mathbf{r}}_i)) = -\frac{\ell(\ell + 1)}{r^2} P_\ell(\hat{\mathbf{r}} \cdot \hat{\mathbf{r}}_i), \quad (33)$$

thus leading to

$$\text{Lap}_s(f(\mathbf{r})) = -\frac{1}{r^2} \sum_{i=1}^N c_i g_{m-1}(\mathbf{r}, \mathbf{r}_i), \quad m > 1, \quad (34)$$

which is known as the *spherical surface Laplacian of $f(\mathbf{r})$* .

In comparison to the previous approach, the method of spherical splines has the advantage of providing a simple expression for the surface Laplacian

of $f(\mathbf{r})$, although it is restricted to spherical geometry only. Additionally, the geodesic distance ensures that the system (26) is non-singular, so that the coefficient d can be determined without using the pseudo-inverse of \mathbf{R} . However, some caution is required. Equation (34) is easy to be implemented, except for the fact that the term $g_{m-1}(\mathbf{r}, \mathbf{r}_i)$ corresponds to an infinite summation. This summation needs to be truncated for evaluation, and truncation error should never be overlooked. The terms that are left out in the truncation of $g_{m-1}(\mathbf{r}, \mathbf{r}_i)$ are Legendre polynomials of higher-degree (large ℓ) that account for high-frequency spatial features. Too much filtering of such features can overcome the potential for improvement in spatial resolution. In view of that, it is important to keep as many Legendre polynomials as possible in the truncated series. Another point worth considering is the factor $(2\ell + 1)/\ell^m(\ell + 1)^m$ that multiplies the Legendre polynomials in equation (31b). This factor falls off as $1/\ell^{2m-1}$. As ℓ increases, it approaches zero rapidly, resulting in a quick cancellation of higher-degree polynomials. The value assigned to m must take this effect into account; the larger the value of m , the more dramatic is the reduction in high-frequency features. Typically, a value of m between 2 and 6 provides satisfactory results for simulation and data analysis (Babiloni et al., 1995; de Barros et al., 2006; Carvalhaes and Suppes, 2011).

3.4. Other approaches

There are many other possible ways to estimate the surface Laplacian of EEG signals. In this section we briefly review the methods proposed by Yao (2002) and Nunez and collaborators (Law et al., 1993a; Nunez and Srinivasan, 2006). Similar to thin-plate splines, Yao’s approach uses interpolation based on radial functions to estimate the surface Laplacian of the potential. The interpolating function has the general form

$$f_{\text{RBF}}(\mathbf{r}) = \sum_{i=1}^N c_i e^{-\frac{m}{\pi^2} S(\mathbf{r}, \mathbf{r}_i)} + b, \quad (35)$$

where $S(\mathbf{r}, \mathbf{r}_j)$ measures the arc of circle connecting \mathbf{r} and \mathbf{r}_i and the parameters c_i and b are subject to

$$f_{\text{RBF}}(\mathbf{r}_i) = V_i, \quad i = 1, \dots, N, \quad (36)$$

where \mathbf{r}_i is the location of the i th electrode and V_i is the value of the potential at that location. Because the system (36) contains $N + 1$ unknowns⁴ but only N equations, it is solved using pseudo-inversion (see the Appendix in Zhai and Yao, 2004).

In contrast to thin-plate splines, the Gaussian function $e^{-\frac{m}{\pi^2} S(\mathbf{r}, \mathbf{r}_i)}$ approaches zero asymptotically with growing the distance from the centers \mathbf{r}_i . The parameter m , commonly referred to as the *spread parameter*, controls

⁴Namely, we have to determine the $N + 1$ parameters c_1, \dots, c_N and d .

the rate of decay of $e^{-\frac{m}{\pi^2}S(\mathbf{r},\mathbf{r}_i)}$. Large values of m produce a sharp decay, resulting in a small range of influence for each node \mathbf{r}_i . Yao recommended to set m according to the number of electrodes in the montage; for instance, $m = 20$ for arrays with 32 sensors, $m = 40$ for 64 sensors, and $m = 50$ for 128 sensors. But he also remarked that a proper choice of m should take into account the source location. In principle, small values of m would be more suitable to fit deep brain sources, whereas shallow sources would be better described by small m -values. In other words, interpolation with Gaussian functions is not automatic. The parameter m needs to be tuned properly for good performance, which can be difficult to achieve for non-equidistant electrodes. Nevertheless, Yao showed consistent results favoring the Gaussian method against spherical splines for simulated and empirical data.

The method developed by Nunez and collaborators is called the *New Orleans Spline-Laplacian* (Law et al., 1993a; Nunez and Srinivasan, 2006). This method uses an interpolating function that resembles two-dimensional splines but with knots in \mathbb{R}^3 instead of \mathbb{R}^2 , i.e.,

$$f_{\text{NOSL}}(\mathbf{r}) = \sum_{i=1}^N c_i |\mathbf{r} - \mathbf{r}_i|^4 \log(|\mathbf{r} - \mathbf{r}_i|^2 + \omega^2) + d_1 + d_2x + d_3y + d_4z + d_5x^2 + d_6xy + d_7xz + d_8y^2 + d_9yz + d_{10}z^2, \quad (37)$$

where the parameters c_i 's and d_i 's are determined in the fashion of equation (26). This method was implemented for spherical and ellipsoidal scalp models and its performance was studied using simulations and real data

(Law et al., 1993a). For ω and z equal to zero it can be proved that $f_{\text{NOSL}}(\mathbf{r})$ is the unique minimizer of (25) in \mathbb{R}^2 (Duchon, 1977; Meinguet, 1979). But f_{NOSL} does not minimize (25) in \mathbb{R}^3 , as the minimizer of (25) in \mathbb{R}^3 is unique and correspond to the spline function (24). Or, putting it in other words, f_{NOSL} is not actually a spline function.⁵ Despite that, Nunez and colleagues reported many studies showing a good performance of their method (Law et al., 1993b; Nunez and Westdorp, 1994; Nunez et al., 2001; Nunez and Srinivasan, 2006) and emphasized its agreement with cortical imaging algorithms in terms of correlation (Nunez et al., 1993, 1994).

3.5. The surface Laplacian matrix

An efficient way of estimating the surface Laplacian of an EEG signal is through a *transformation matrix*. A matrix transformation for the surface Laplacian differentiation is a mapping from an instantaneous distribution $\mathbf{v} = (V_1, \dots, V_N)$ into $\text{Lap}_S(\mathbf{v})$. That is, the surface Laplacian of \mathbf{v} corresponds to the product $\mathbf{L}\mathbf{v}$, where \mathbf{L} is the surface Laplacian transformation matrix. A major advantage of this procedure over direct calculations is that the same matrix \mathbf{L} can be used to transform data from different individuals and experiments, requiring only that the electrode locations and scalp model remain the same.

⁵Due to the constraint (30), the NOSL algorithm is also affected by the singularity of (26) on spherical and ellipsoidal scalp models (see discussion in Section 3.2). Apparently, in a effort to remedy this problem the Matlab code of Nunez and Srinivasan (2006, p. 585) adds “noise” (error) to zero-valued electrode coordinates, effectively making (26) nonsingular, but not necessarily leading to well-conditioned solutions.

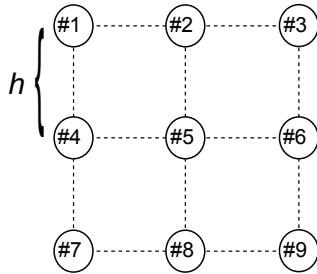


Figure 5: A montage with 9 electrodes in a square grid of spacing h . The numbers 1 to 9 identify the electrodes and should not be confused with the weights for a finite difference approximation.

Let us first consider the case of finite difference approximations, for which \mathbf{L} can be constructed row by row using the stencils of Figure 3; electrodes that do not contribute to the transformation of a data point are assigned a zero weight. This way, each row of \mathbf{L} has as many elements as the number of channels in the montage, but only five elements are nonzero in each row. This implies that \mathbf{L} will be a sparse matrix, with sparsity increasing with the number of channels. Because the weights of each stencil sum to zero, the columns of \mathbf{L} also sum to zero, reflecting the fact that the transformation is reference-free.

As a simple illustration, consider the fictitious arrangement of Figure 5, with 9 electrodes evenly distributed in a square grid of spacing h . The \mathbf{L} matrix for this arrangement has dimension 9×9 . Using the stencils of

Figure 3, we obtain

$$\mathbf{L} = \frac{1}{h^2} \begin{pmatrix} 2 & -2 & 1 & -2 & 0 & 0 & 1 & 0 & 0 \\ 1 & -1 & 1 & 0 & -2 & 0 & 0 & 1 & 0 \\ 1 & -2 & 2 & 0 & 0 & -2 & 0 & 0 & 1 \\ 1 & 0 & 0 & -1 & -2 & 1 & 1 & 0 & 0 \\ 0 & 1 & 0 & 1 & -4 & 1 & 0 & 1 & 0 \\ 0 & 0 & 1 & 1 & -2 & -1 & 0 & 0 & 1 \\ 1 & 0 & 0 & -2 & 0 & 0 & 2 & -2 & 1 \\ 0 & 1 & 0 & 0 & -2 & 0 & 1 & -1 & 1 \\ 0 & 0 & 1 & 0 & 0 & -2 & 1 & -2 & 2 \end{pmatrix}. \quad (38)$$

A quick inspection shows that all diagonal elements of \mathbf{L} are nonzero. But they add to zero, implying that \mathbf{L} *does not possess inverse*. The inability to invert \mathbf{L} is a general property of the surface Laplacian technique that reflects the ambiguity on the choice of reference. Stated in other words, a Laplacian transformation $\mathbf{L}\mathbf{v}$ cannot be uniquely undone.

Grid-free methods generate \mathbf{L} matrices that are non-sparse. In the context of smoothing splines, Carvalhaes and Suppes (2011) showed that

$$\mathbf{L}_\lambda = \tilde{\mathbf{K}}\mathbf{C}_\lambda + \tilde{\mathbf{T}}\mathbf{D}_\lambda, \quad (39)$$

where the subscript emphasizes dependency on the smoothing parameter,

and

$$(\tilde{\mathbf{K}})_{ij} = \text{Lap}_s (|\mathbf{r}_i - \mathbf{r}_j|^{2m-3}), \quad (40a)$$

$$(\tilde{\mathbf{T}})_{ij} = \text{Lap}_s (\nu_i(\mathbf{r}_j)), \quad (40b)$$

$$\mathbf{C}_\lambda = \mathbf{Q}_2 [\mathbf{Q}'_2 (\mathbf{K} + N\lambda\mathbf{I}) \mathbf{Q}_2]^{-1} \mathbf{Q}'_2, \quad (40c)$$

$$\mathbf{D}_\lambda = \mathbf{R}^+ \mathbf{Q}'_1 (\mathbf{1} - \mathbf{K}\mathbf{C}_\lambda - N\lambda\mathbf{C}_\lambda). \quad (40d)$$

As expected, these expressions clearly show that \mathbf{L}_λ depends on the electrode coordinates and λ , but not on the potential distribution. Because $\text{Lap}_s (\nu_i(\mathbf{r}_j))$ vanishes for any polynomial ν_i of degree less than 2, the first four columns of $\tilde{\mathbf{T}}$ are always null, which is sufficient to prove that \mathbf{L}_λ does not allow unambiguous inverse operation.

3.6. Regularization of smoothing splines

The smoothing spline function depends on two free parameters, m and λ . This section focuses on the determination of λ . The λ parameter controls the trade-off between a good fit and the smoothness of $f_\lambda(\mathbf{r})$. With $\lambda > 0$ the spline function fits the data points closely but not exactly, resulting in a smooth waveform that contains less variance than that for $\lambda = 0$. In other words, with $\lambda > 0$ the estimate $f_\lambda(\mathbf{r})$ is *biased*. It turns out that some degree of bias is not only tolerable but also desirable. This is because EEG data are usually affected by spatial noise, which increases variance and tends to be amplified by Laplacian differentiation. Smoothing the data

reduces this problem, but too much bias can lead to loss of important information. Therefore, a good criterion for a suitable choice of λ is crucial. For this purpose, Craven and Wahba (1979) developed the method of *generalized cross-validation*. Basically, the GCV criterion is an optimization procedure which consists of minimizing the error function

$$\text{CGV}(f_\lambda) = \frac{1}{N} \sum_{i=1}^N \left[\frac{V_i - f_\lambda(\mathbf{r}_i)}{1 - \text{trace}(\mathbf{S}_\lambda)/N} \right]^2, \quad (41)$$

where $\mathbf{v} = (V_1, \dots, V_N)$ is the given potential distribution and \mathbf{S}_λ is an associated *smoother matrix*. The smoother matrix transforms an input \mathbf{v} into a smooth waveform \mathbf{v}_λ , according to

$$\mathbf{v}_\lambda = \mathbf{S}_\lambda \mathbf{v}, \quad (42)$$

where $\mathbf{S}_\lambda = \mathbf{K} \mathbf{C}_\lambda + \mathbf{T} \mathbf{D}_\lambda$. This expression is general and follows directly from (24), using matrix notation and applying the definitions of \mathbf{C}_λ and \mathbf{D}_λ given in equations (40). The smoother matrix has dimension $N \times N$ and does not involve differentiation. Because of the later, and in contrast to \mathbf{L}_λ , it is easily computable for any scalp model.

The trace operation in (42) sums over the diagonal elements of \mathbf{S}_λ and results in a real number between 2 and N . In statistics, this number is interpreted as the *effective degree of freedom* of the smoothing spline function (Hastie et al., 2009; James et al., 2013). This interpretation is useful because

it gives a sense of how much bias is being applied: the higher the degree of freedom, the less biased the estimate. Note that because (41) is singular at $\lambda = 0$, which leads to $\text{trace}(\mathbf{S}_0) = N$, the CGV algorithm excludes the possibility of having $\lambda = 0$ as optimal value.

An application of the GCV statistics in the choice of λ is illustrated in Figure 6. The data used in this example are included in the distribution of the EEGLab Matlab Toolbox, version 13.2.2b (Delorme and Makeig, 2004). A dataset included in this distribution which was available to us contains 30,504 frames recorded from 32 channels at a sampling rate of 128 Hz, from which we arbitrarily selected the frame of number 500. The optimal degree of freedom of $f_\lambda(\mathbf{r})$ was 22.85, much lower than the value of 32 corresponding to $\lambda = 0$. This result was obtained computing the \mathbf{S}_λ matrix 1,000 times, with λ varying from 10^{-16} to 10^3 on a log scale.

Unfortunately, there seems to be no simple way of estimating the optimal degree of freedom for multiple frames without repeating the minimization procedure several times. Depending on the dataset, this is not only impractical but also undesirable to avoid drastic changes in the smoothing parameter across successive time frames. The exhaustive search for the best λ over a set of preselected values for the whole dataset is an option that carries a high computational cost (Babiloni et al., 1995). But we can proceed as follows. Split the data into small chunks, and for each chunk randomly select a frame to search for the optimal degree of freedom. Assign this result to the whole chunk, reducing the number of computations to the number

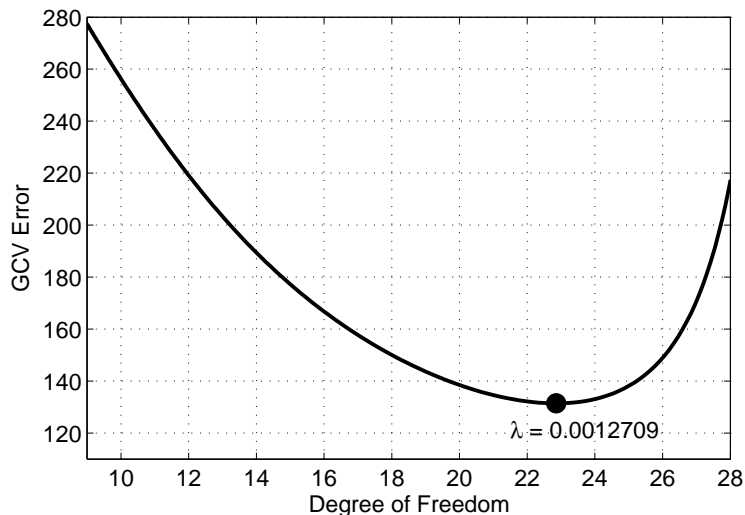


Figure 6: An application of the GCV algorithm to determine the optimal λ . The error curve reaches its minimum value for an effective degree of freedom of 22.85, which corresponded to $\lambda = 0.0012709$.

of chunks instead of the number of frames. Assuming that the optimal degree of freedom does not change substantially over a small time interval, this procedure should be quite acceptable in general. As an example, Figure 7 shows averages and standard deviations of the optimal degree of freedom over 100-ms intervals, where the data corresponded to the first 3,000 ms of the aforementioned EEGLab dataset. For most of this 3,000-ms segment the optimal degree of freedom predicted by GCV did not change substantially over 100-ms intervals, suggesting that the random choice of a time sample within each chunk could, in fact, provide satisfactory results.

Alternatively, we could think of using 4-D splines to smooth small chunks of data, taking time as a fourth coordinate. But even for small chunks the resulting smoother matrix could be too large to provide reliable results due

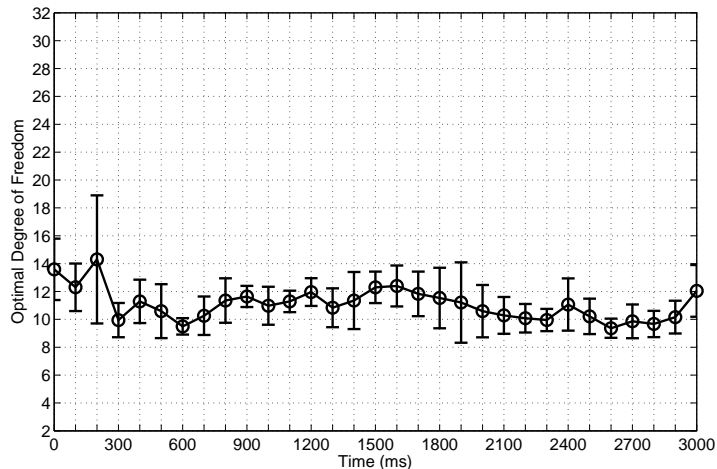


Figure 7: Mean and standard deviation of the optimal degree of freedom over 100-ms intervals.

to ill-conditioning. For instance, each chunk in Figure 7 contained 13 frames, leading to a smoother matrix of dimension 416×416 . Increasing the number of electrodes to 128 would enlarge \mathbf{S}_λ to 1664×1664 , which is too large to work well in practice.

4. Concluding Remarks

The surface Laplacian technique is an extensive subject of research, and this paper could only partially review or expand a few topics of particular interest. For instance, it was outside the scope of our work to discuss computational methods based on the actual geometry of the head, as they require specialized tools that are often not readily available to most researchers, and the interested reader is referred to Le and Gevins (1993); Gevins et al. (1994); Le et al. (1994); Babiloni et al. (1996).

Another important topic not covered here is related to the size of actual electrodes. Since measuring electrodes have finite size, EEG recordings should be interpreted as spatial averages (subject to special boundary conditions) instead of point values. However, all approaches discussed in this paper were originally built upon the idea of a point-like electrode. An extensive discussion of this matter is outside the scope of this paper as well. But let us briefly sketch a possible way to approach it, by recalling that a similar problem occurs in the approximation of a histogram by a continuous function (the density function), which has led to the concept of *histopolatation* (Boneva et al., 1971; Wahba, 1976). The basic idea to deal with this problem is quite simple and consists of replacing the interpolation condition $V_i = f(\mathbf{r}_i)$ with the *volume matching condition* $V_i = \iint_{\Omega_i} f(\mathbf{r}_i) dA$ in the spline framework, the double integral being taken over the area of an electrode. This modification turns the variational problem of minimizing (25) into the problem of minimizing

$$\text{RSS}(f, \lambda) = \frac{1}{N} \sum_i \left[V_i - \iint_{\Omega_i} f(\mathbf{r}_i) dA \right]^2 + \lambda J_m[f]. \quad (43)$$

Wahba (1981) studied a solution to this problem in Euclidean space and used the GCV statistics to estimate the smoothing parameter λ . A similar solution could be sought here, but possibly adopting spherical coordinates to express the geometry of the electrodes in a way to simplify calculations. This problem can be difficult to solve analytically and it is almost certain

that a numerical solution is required.

It would be also interesting to address possible approaches going beyond the surface Laplacian technique. Along this line, we recently reported a successful attempt to further improve EEG classification by jointly using the surface Laplacian of the potential and the tangential components of the scalp electric field (Wang et al., 2012; Carvalhaes et al., 2014). This approach was grounded on the fact that the surface Laplacian derivation is closely related to the component of the electric field normal to the scalp surface, thus not containing substantial information about features encoded in tangential direction. Not surprisingly, this combination of physically distinct but somewhat supplementary quantities resulted in significant improvement for a variety of classification tasks.

Appendix A. The Mathematics Behind Finite Difference

A systematic way to obtain finite difference approximations for the derivatives of a function is based on the *Taylor series expansion*. For mathematical reasons, we will formulate the problem in terms of a continuous function V and then, for compatibility with our notation in Section 3.1, rewrite the final approximation using discrete variables. In its simplest case, the Taylor series of a univariate function $V(x)$ around a point $x = a$ is defined by the infinite summation

$$V(a + h) = V(a) + V'(a)h + \frac{1}{2!}V''(a)h^2 + \frac{1}{3!}V'''(a)h^3 + \dots, \quad (\text{A.1})$$

where h is called the increment, $n! = n(n-1)(n-2)\cdots 1$ is the factorial of n , and $V^{(n)}(a)$ denotes the n -th derivative of $V(x)$ at $x = a$. That is, the Taylor series of $V(x)$ is a power series of h with coefficients given by the derivatives of $V(x)$ at $x = a$. To obtain an approximation for the second derivative (or any other derivative) of $V(x)$ at $x = a$ we proceed as follows. Replace h with $-h$ in (A.1) and obtain an analogous expression for $V(a-h)$, i.e.,

$$V(a-h) = V(a) - V'(a)h + \frac{1}{2!}V''(a)h^2 - \frac{1}{3!}V'''(a)h^3 + \cdots$$

Adding these two expressions,

$$V(a+h) + V(a-h) = 2V(a) + V''(a)h^2 + \frac{1}{12}V^{iv}(a)h^4 + \cdots,$$

whence

$$V''(a) = \frac{V(a+h) + V(a-h) - 2V(a)}{h^2} - \frac{1}{12}V^{iv}(a)h^2 - \cdots, \quad (\text{A.2})$$

Assuming that h is sufficiently small we can ignore all terms containing powers of h and arrive at

$$V''(a) \approx \frac{V(a+h) + V(a-h) - 2V(a)}{h^2}.$$

Replacing $a = (i - 1)h$, $i = 2, \dots, N - 1$, and using the notation $V_i = V(a)$ and $V_{i\pm 1} = V(a \pm h)$ yields

$$V''(a) \approx \frac{V_{i+1} + V_{i-1} - 2V_i}{h^2}. \quad (\text{A.3})$$

This expression was obtained by truncating the infinite series (A.2) after the first term. This way, starting from h^2 all powers of h were eliminated assuming that h was sufficiently small. The result was a *second-order approximation*⁶, which in the “big-Oh” notation is referred to as $\mathcal{O}(h^2)$.

Approximation (A.3) excludes the case of a peripheral node, for which either V_{i+1} or V_{i-1} does not exist. In this case, we have to build the approximation using only nodes to the right or left of a , but not both. For instance, let $i = 1$ and use the expansions

$$\begin{aligned} V(a + h) &= V(a) + V'(a)h + \frac{1}{2}V''(a)h^2 + \frac{1}{6}V'''(a)h^3 + \dots, \\ V(a + 2h) &= V(a) + 2V'(a)h + 2V''(a)h^2 + \frac{4}{3}V'''(a)h^3 + \dots, \end{aligned}$$

from which

$$V(a + 2h) - 2V(a + h) = -V(a) + V''(a)h^2 + V'''(a)h^3 + \dots$$

⁶The order of a finite difference approximation is given by the smallest power of h that is left out in the truncation.

and

$$V''(a) = \frac{V(a+2h) - 2V(a+h) + V(a)}{h^2} - V'''(a)h - \dots$$

In terms of the grid variables,

$$V''(a) \approx \frac{V_3 - 2V_2 + V_1}{h^2}, \quad (\text{A.4})$$

which is a *first order approximation*.

Appendix A.1. Bivariate functions and approximations for $\text{Lap}(V(a, b))$

The extension of (A.1) to bivariate functions replaces ordinary derivatives with partial derivatives. Namely,

$$\begin{aligned} V(a+h_1, b+h_2) = & V(a, b) + \left[\frac{\partial V(a, b)}{\partial x} h_1 + \frac{\partial V(a, b)}{\partial y} h_2 \right] + \frac{1}{2} \left[\frac{\partial^2 V(a, b)}{\partial x^2} h_1^2 + 2 \frac{\partial^2 V(a, b)}{\partial x \partial y} h_1 h_2 \right. \\ & \left. + \frac{\partial^2 V(a, b)}{\partial y^2} h_2^2 \right] + \frac{1}{6} \left[\frac{\partial^3 V(a, b)}{\partial x^3} h_1^3 + 3 \frac{\partial^3 V(a, b)}{\partial^2 x \partial y} h_1^2 h_2 + 3 \frac{\partial^3 V(a, b)}{\partial x \partial^2 y} h_1 h_2^2 + \frac{\partial^3 V(a, b)}{\partial y^3} h_2^3 \right] + \dots \end{aligned} \quad (\text{A.5})$$

Similar to the one-dimensional case, with appropriate choices for h_1 and h_2 one can use this expansion to approximate the partial derivatives of $V(x, y)$ at any point in a rectangular grid. An approximation for the Laplacian of $V(x, y)$ at a central node of a square grid ($h_1 = h_2 = h$) is obtained as follows.

First, use (A.5) to expand $V(a \pm h, b)$ and $V(a, b \pm h)$:

$$\begin{aligned} V(a \pm h, b) &= V(a, b) \pm \frac{\partial V(a, b)}{\partial x} h + \frac{1}{2} \frac{\partial^2 V(a, b)}{\partial x^2} h^2 \pm \frac{1}{6} \frac{\partial^3 V(a, b)}{\partial x^3} h^3 + \frac{1}{24} \frac{\partial^4 V(a, b)}{\partial x^4} h^4 \pm \dots, \\ V(a, b \pm h) &= V(a, b) \pm \frac{\partial V(a, b)}{\partial y} h + \frac{1}{2} \frac{\partial^2 V(a, b)}{\partial y^2} h^2 \pm \frac{1}{6} \frac{\partial^3 V(a, b)}{\partial y^3} h^3 + \frac{1}{24} \frac{\partial^4 V(a, b)}{\partial y^4} h^4 + \dots. \end{aligned}$$

Second, add these four expressions to obtain

$$\begin{aligned} V(a+h, b) + V(a-h, b) + V(a, b+h) + V(a, b-h) &= 4V(a, b) + \underbrace{\left[\frac{\partial^2 V(a, b)}{\partial x^2} + \frac{\partial^2 V(a, b)}{\partial y^2} \right]}_{=\text{Lap}(V(a, b))} h^2 \\ &+ \frac{1}{12} \left[\frac{\partial^4 V(a, b)}{\partial x^4} + \frac{\partial^4 V(a, b)}{\partial y^4} \right] h^4 + \dots, \end{aligned}$$

whence

$$\text{Lap}(V(a, b)) = \frac{V(a+h, b) + V(a-h, b) + V(a, b+h) + V(a, b-h) - 4V(a, b)}{h^2} + \mathcal{O}(h^2).$$

Therefore, $\text{Lap}(V(a, b))$ is approximated to the second-order of h by

$$\text{Lap}(V(a, b)) \approx \frac{V(a+h, b) + V(a-h, b) + V(a, b+h) + V(a, b-h) - 4V(a, b)}{h^2}.$$

This expression is equivalent to the approximation (20) with $V_{(i,j)} = V(a, b)$,

$V_{(i\pm 1, j)} = V(a, b \mp h)$, and $V_{(i, j\pm 1)} = V(a \pm h, b)$.

Appendix A.2. Approximations for peripheral electrodes

Suppose that we want to approximate $\text{Lap}(V)$ at a point (a, b) which is outside the domain of V . Let us start with a node in the left border of the grid, but not in a corner. Our mapping from the continuous variables x and y into the discrete variables i and j follows $x = (j - 1)h$ and $y = (N - i + 1)h$. See also the scheme in Figure 2. For a node on the left border $x = 0$, which corresponds to the first column of the grid ($j = 1$). The Taylor series of interest are

$$\begin{aligned} V(h, b) &= V(0, b) + \frac{\partial V(0, b)}{\partial x}h + \frac{1}{2}\frac{\partial^2 V(0, b)}{\partial x^2}h^2 + \frac{1}{6}\frac{\partial^3 V(0, b)}{\partial x^3}h^3 + \frac{1}{24}\frac{\partial^4 V(0, b)}{\partial x^4}h^4 + \dots, \\ V(2h, b) &= V(0, b) + 2\frac{\partial V(0, b)}{\partial x}h + 2\frac{\partial^2 V(0, b)}{\partial x^2}h^2 + \frac{4}{3}\frac{\partial^3 V(0, b)}{\partial x^3}h^3 + \frac{2}{3}\frac{\partial^4 V(0, b)}{\partial x^4}h^4 + \dots, \\ V(0, b \pm h) &= V(0, b) \pm \frac{\partial V(0, b)}{\partial y}h + \frac{1}{2}\frac{\partial^2 V(0, b)}{\partial y^2}h^2 \pm \frac{1}{6}\frac{\partial^3 V(0, b)}{\partial y^3}h^3 + \frac{1}{24}\frac{\partial^4 V(0, b)}{\partial y^4}h^4 \pm \dots. \end{aligned}$$

A linear combination of these expansions with weights $-2, 1, 1,$ and 1 gives

$$\begin{aligned} -2V(h, b) + V(2h, b) + V(0, b+h) + V(0, b-h) &= V(0, b) + \underbrace{\left[\frac{\partial^2 V(0, b)}{\partial x^2} + \frac{\partial^2 V(0, b)}{\partial y^2} \right]}_{=\text{Lap}(V(0, b))} h^2 \\ &\quad + \frac{\partial^3 V(0, b)}{\partial x^3} h^3 + \dots, \end{aligned}$$

so that

$$\text{Lap}(V(0, b)) = \frac{-2V(h, b) + V(2h, b) + V(0, b+h) + V(0, b-h) - V(0, b)}{h^2} - \frac{\partial^3 V(0, b)}{\partial x^3} h.$$

Assuming that h is sufficiently small we obtain

$$\text{Lap}(V(0, b)) \approx \frac{V(2h, b) - 2V(h, b) + V(0, b + h) + V(0, b - h) - V(0, b)}{h^2},$$

which is a *first-order approximation*. In terms of the grid variables,

$$\text{Lap}(V)|_{(i,1)} \approx \frac{V_{(i,3)} - 2V_{(i,2)} + V_{(i-1,1)} + V_{(i+1,1)} - V_{(i,1)}}{h^2}, \quad (\text{A.8a})$$

In a similar fashion, for grid points at right, bottom, and upper edges (excluding the corners) we obtain, respectively,

$$\text{Lap}(V)|_{(i,N)} \approx \frac{V_{(i,N-2)} - 2V_{(i,N-1)} + V_{(i-1,N)} + V_{(i+1,N)} - V_{(i,N)}}{h^2}, \quad (\text{A.8b})$$

$$\text{Lap}(V)|_{(N,j)} \approx \frac{V_{(N-2,j)} - 2V_{(N-1,j)} + V_{(N,j-1)} + V_{(N,j+1)} - V_{(N,j)}}{h^2} \quad (\text{A.8c})$$

$$\text{Lap}(V)|_{(1,j)} \approx \frac{V_{(3,j)} - 2V_{(2,j)} + V_{(1,j-1)} + V_{(1,j+1)} - V_{(1,j)}}{h^2} \quad (\text{A.8d})$$

Finally, assume that the node of interest is at the left upper corner of the grid, corresponding to $i = j = 1$ ($a = 0$, $b = (N - 1)h$). To approximate the Laplacian of V at this node we use

$$\begin{aligned} V(h, b) &= V(0, b) + \frac{\partial V(0, b)}{\partial x} h + \frac{1}{2} \frac{\partial^2 V(0, b)}{\partial x^2} h^2 + \frac{1}{6} \frac{\partial^3 V(0, b)}{\partial x^3} h^3 + \frac{1}{24} \frac{\partial^4 V(0, b)}{\partial x^4} h^4 + \dots, \\ V(2h, b) &= V(0, b) + 2 \frac{\partial V(0, b)}{\partial x} h + 2 \frac{\partial^2 V(0, b)}{\partial x^2} h^2 + \frac{4}{3} \frac{\partial^3 V(0, b)}{\partial x^3} h^3 + \frac{2}{3} \frac{\partial^4 V(0, b)}{\partial x^4} h^4 + \dots, \\ V(0, b - 2h) &= V(0, b) - 2 \frac{\partial V(0, b)}{\partial y} h + 2 \frac{\partial^2 V(0, b)}{\partial y^2} h^2 - \frac{2}{3} \frac{\partial^3 V(0, b)}{\partial y^3} h^3 + \frac{2}{3} \frac{\partial^4 V(0, b)}{\partial y^4} h^4 + \dots, \\ V(0, b - h) &= V(0, b) - \frac{\partial V(0, b)}{\partial y} h + \frac{1}{2} \frac{\partial^2 V(0, b)}{\partial y^2} h^2 - \frac{1}{6} \frac{\partial^3 V(0, b)}{\partial y^3} h^3 + \frac{1}{24} \frac{\partial^4 V(0, b)}{\partial y^4} h^4 + \dots. \end{aligned}$$

Adding these expansions with weights -2 , 1 , 1 , and -2 yields

$$\begin{aligned}
-2V(h, b) + V(2h, b) + V(0, b-2h) - 2V(0, b-h) &= -2V(0, b) + \underbrace{\left[\frac{\partial^2 V(0, b)}{\partial x^2} + \frac{\partial^2 V(0, b)}{\partial y^2} \right]}_{=\text{Lap}(V(a,b))} h^2 \\
&+ \left[\frac{\partial^3 V(0, b)}{\partial x^3} - \frac{\partial^3 V(0, b)}{\partial y^3} \right] h^3 + \dots
\end{aligned}$$

Solving for $\text{Lap}(V)$ we obtain the first-order approximation

$$\text{Lap}(V(0, b)) \approx \frac{V(2h, b) - 2V(h, b) + V(0, b-2h) - 2V(0, b-h) + 2V(0, b)}{h^2}.$$

Equivalently,

$$\text{Lap}(V)|_{(1,1)} \approx \frac{V_{(1,3)} - 2V_{(1,2)} + V_{(3,1)} - 2V_{(2,1)} + 2V_{(1,1)}}{h^2}. \quad (\text{A.10})$$

Using symmetry we can obtain similar approximations for the other corners of the grid illustrated in Figure 3.

References

- Abramowitz, M., Stegun, I. A., 1964. Handbook of mathematical functions: with formulas, graphs, and mathematical tables. Dover Publications, Inc., New York.
- Alschuler, D. M., Tenke, C. E., Bruder, G. E., Kayser, J., 2014. Identifying electrode bridging from electrical distance distributions: a survey of

- publicly-available EEG data using a new method. *Clin. Neurophysiol.* 125, 484–490.
- Astolfi, L., Cincotti, F., Mattia, D., Marciani, M. G., Baccala, L. A., de Vico Fallani, F., Salinari, S., Ursino, M., Zavaglia, M., Ding, L., Edgar, J. C., Miller, G. A., He, B., Babiloni, F., 2007. Comparison of different cortical connectivity estimators for high-resolution EEG recordings. *Hum. Brain Mapp.* 28, 143–157.
- Babiloni, F., Babiloni, C., Carducci, F., Fattorini, L., Onorati, P., Urbano, A., 1996. Spline Laplacian estimate of EEG potentials over a realistic magnetic resonance-constructed scalp surface model. *Electroencephalogr. Clin. Neurophysiol.* 98, 363–373.
- Babiloni, F., Babiloni, C., Fattorini, L., Carducci, F., Onorati, P., Urbano, A., 1995. Performances of surface Laplacian estimators: A study of simulated and real scalp potential distributions. *Brain Topogr.* 8, 35–45.
- Boneva, L. I., Kendall, D. G., Stefanov, I., 1971. Spline transformations: Three new diagnostic aids for statistical data-analyst. *J. Royal Statist. Soc. Ser. B* 33, 1–70.
- Carvalhoes, C., 2013. Spline interpolation on nonunisolvent sets. *IMA J. Num. Anal.* 33, 370–375.
- Carvalhoes, C., Perreau-Guimaraes, M., Grosenick, L., Suppes, P., 2009.

- EEG classification by ICA source selection of Laplacian-filtered data. In: Proc. IEEE ISBI 09. pp. 1003–1006.
- Carvalhoes, C. G., de Barros, J. A., Perreau-Guimaraes, M., Suppes, P., 2014. The joint use of the tangential electric field and surface Laplacian in EEG classification. *Brain Topogr.* 27, 84–94.
- Carvalhoes, C. G., Suppes, P., Nov 2011. A spline framework for estimating the EEG surface laplacian using the Euclidean metric. *Neural Comput.* 23 (11), 2974–3000.
- Craven, P., Wahba, G., 1979. Smoothing noisy data with spline functions: Estimating the correct degree of smoothing by the method of generalized cross-validation. *Numer Math*, 377–403.
- de Barros, J. A., Carvalhoes, C., de Mendonça, J. P. R. F., Suppes, P., 2006. Recognition of words from the EEG Laplacian. *Braz. J. Biom. Eng.* 21, 45–59.
- Del Percio, C., Brancucci, A., Bergami, F., Marzano, N., Fiore, A., Di Ciolo, E., Aschieri, P., Lino, A., Vecchio, F., Iacoboni, M., Gallamini, M., Babiloni, C., Eusebi, F., 2007. Cortical alpha rhythms are correlated with body sway during quiet open-eyes standing in athletes: a high-resolution EEG study. *Neuroimage* 36, 822–829.
- Delorme, A., Makeig, S., 2004. EEGLAB: an open source toolbox for analysis

- of single-trial EEG dynamics including independent component analysis. *J. Neurosci. Meth.* 134, 9–21.
- Doesburg, S. M., Roggeveen, A. B., Kitajo, K., Ward, L. M., 2008. Large-scale gamma-band phase synchronization and selective attention. *Cereb. Cortex* 18, 386–396.
- Duchon, J., 1977. Splines minimizing rotation-invariant semi-norms in Sobolev spaces. In: *Constructive theory of functions of several variables*. Vol. 571. pp. 85–100.
- Eubank, R. L., 1999. *Nonparametric regression and spline smoothing*, 2nd Edition. Vol. 157 of *Statistics: textbooks and monographs*. Marcel Dekker, New York.
- Fitzgibbon, S. P., Lewis, T. W., Powers, D. M., Whitham, E. W., Willoughby, J. O., Pope, K. J., 2013. Surface Laplacian of central scalp electrical signals is insensitive to muscle contamination. *IEEE Trans. Biom. Eng.* 60, 4–9.
- Freeman, J. A., Nicholson, C., 1975. Experimental optimization of current source-density technique for anuran cerebellum. *J. Neurophysiol.* 38, 369–382.
- Gevins, A., 1988. *Dynamics of Sensory and Cognitive Processing of the Brain*. Springer-Verlag, Ch. Recent advances in neurocognitive pattern analysis, pp. 88–102.

- Gevins, A., 1989. Dynamic functional topography of cognitive tasks. *Brain Topogr.* 2, 37–56.
- Gevins, A., Brickett, P., Costales, B., Le, J., Reutter, B., 1990. Beyond topographic mapping: towards functional-anatomical imaging with 124-channel EEGs and 3-D MRIs. *Brain Topogr.* 3, 53–64.
- Gevins, A., Le, J., Martin, N. K., Brickett, P., Desmond, J., Reutter, B., 1994. High resolution EEG: 124-channel recording, spatial deblurring and MRI integration methods. *Electroencephalogr. Clin. Neurophysiol.* 90, 337–58.
- Green, P. J., Silverman, B. W., 1994. Nonparametric regression and generalized linear models: a roughness penalty approach. *Monographs on Statistics & Applied Probability*. Chapman & Hall, London.
- Greischar, L. L., Burghy, C. A., van Reekum, C. M., Jackson, D. C., Pizzagalli, D. A., Mueller, C., Davidson, R. J., 2004. Effects of electrode density and electrolyte spreading in dense array electroencephalographic recording. *Clin. Neurophysiol.* 115, 710–720.
- Hämäläinen, M., Hari, R., Ilmoniemi, R. J., Knuutila, J., Lounasmaa, O. V., 1993. Magnetoencephalography—theory, instrumentation, and applications to noninvasive studies of the working human brain. *Rev. Mod. Phys.* 65, 413–497.

- Hastie, T., Tibshirani, R., Friedman, J., Hastie, T., Friedman, J., Tibshirani, R., 2009. *The Elements of Statistical Learning: Data Mining, Inference, and Prediction*. Springer Series in Statistics. Springer, New York.
- Hjorth, B., 1975. An on-line transformation of EEG scalp potentials into orthogonal source derivations. *Electroencephalogr. Clin. Neurophysiol.* 39, 526–530.
- Jackson, J. D., 1999. *Classical Electrodynamics*, 3rd ed. Wiley, New York.
- James, G., Witten, D., Hastie, T., Tibshirani, R., 2013. *An Introduction to Statistical Learning with Applications in R*. Springer Texts in Statistics. Springer, New York.
- Kayser, J., Tenke, C. E., 2006a. Principal components analysis of Laplacian waveforms as a generic method for identifying ERP generator patterns: I. evaluation with auditory oddball tasks. *Clin. Neurophysiol.* 117, 348–368.
- Kayser, J., Tenke, C. E., 2006b. Principal components analysis of Laplacian waveforms as a generic method for identifying ERP generator patterns: II. adequacy of low-density estimates. *Clin. Neurophysiol.* 117, 369–380.
- Law, S. K., Nunez, P. L., Wijesinghe, R. S., 1993a. High-resolution EEG using spline generated surface Laplacians on spherical and ellipsoidal surfaces. *IEEE Trans. Biom. Eng.* 40, 145–153.
- Law, S. K., Rohrbaugh, J. W., Adams, C. M., Eckardt, M. J., 1993b. Im-

- proving spatial and temporal resolution in evoked EEG responses using surface Laplacians. *Electroencephalogr. Clin. Neurophysiol.* 88, 309–322.
- Le, J., Gevins, A., 1993. Method to reduce blur distortion from EEG's using a realistic head model. *IEEE Trans. Biom. Eng.* 40, 517–528.
- Le, J., Menon, V., Gevins, A., 1994. Local estimate of surface Laplacian derivation on a realistically shaped scalp surface and its performance on noisy data. *Electroencephalogr. Clin. Neurophysiol.* 92, 433–441.
- McFarland, D. J., McCane, L. M., David, S. V., Wolpaw, J. R., 1997. Spatial filter selection for EEG-based communication. *Electroencephalogr. Clin. Neurophysiol.* 103, 386–394.
- Meinguet, J., 1979. Multivariate interpolation at arbitrary points made simple. *J. App. Math. Phys.* 30, 292–304.
- Müller-Gerking, J., Pfurtscheller, G., Flyvbjerg, H., 1999. Designing optimal spatial filters for single-trial EEG classification in a movement task. *Clin. Neurophysiol.* 110, 787–798.
- Nicholson, C., 1973. Theoretical analysis of field potentials in anisotropic ensembles of neuronal elements. *IEEE Trans. Biomed. Eng.* 20, 278–288.
- Nicholson, C., Freeman, J. A., 1975. Theory of current source-density analysis and determination of conductivity tensor for anuran cerebellum. *J. Neurophysiol.* 38, 356–368.

- Nunez, P. L., Silberstein, R. B., Cadusch, P. J., Wijesinghe, R., 1993. Comparison of high resolution EEG methods having different theoretical bases. *Brain Topogr.* 5, 361–364.
- Nunez, P. L., Silberstein, R. B., Cadusch, P. J., Wijesinghe, R. S., Westdorp, A. F., Srinivasan, R., 1994. A theoretical and experimental study of high resolution EEG based on surface laplacians and cortical imaging. *Electroencephalogr. Clin. Neurophysiol.* 90, 40–57.
- Nunez, P. L., Srinivasan, R., 2006. *Electric Fields of the Brain: The Neurophysics of EEG*, 2nd Edition. Oxford University Press, New York.
- Nunez, P. L., Westdorp, A. F., 1994. The surface Laplacian, high-resolution EEG and controversies. *Brain Topogr.* 6, 221–226.
- Nunez, P. L., Wingeier, B. M., Silberstein, R. B., 2001. Spatial-temporal structures of human alpha rhythms: Theory, microcurrent sources, multiscale measurements, and global binding of local networks. *Hum. Brain Mapp.* 13, 125–164.
- Perrin, F., Pernier, J., Bertrand, O., Echallier, J. F., 1989. Spherical splines for scalp potential and current density mapping. *Electroencephalogr. Clin. Neurophysiol.* 72, 184–187.
- Schey, H. M., 2004. *Div, Grad, Curl, And All That: An Informal Text On Vector Calculus*. W. W. Norton & Company.

- Sibson, R., Stone, G., 1991. Computation of thin-plate splines. *SIAM J. Sci. Stat. Comput.* 12, 1304–1313.
- Srinivasan, R., Winter, W. R., Ding, J., Nunez, P. L., 2007. EEG and MEG coherence: measures of functional connectivity at distinct spatial scales of neocortical dynamics. *J. Neurosci. Meth.* 166, 41–52.
- Tenke, C. E., Kayser, J., 2001. A convenient method for detecting electrolyte bridges in multichannel electroencephalogram and event-related potential recordings. *Clin. Neurophysiol.* 112, 545–550.
- Tenke, C. E., Kayser, J., 2012. Generator localization by current source density (CSD): implications of volume conduction and field closure at intracranial and scalp resolutions. *Clin. Neurophysiol.* 123, 2328–2345.
- Tenke, C. E., Kayser, J., Fong, R., Leite, P., Towey, J. P., Bruder, G. E., 1998. Response- and stimulus-related ERP asymmetries in a tonal oddball task: a Laplacian analysis. *Brain Topogr.* 10, 201–210.
- Tenke, C. E., Schroeder, C. E., Arezzo, J. C., Vaughan, Jr, H., 1993. Interpretation of high-resolution current source density profiles: a simulation of sublaminal contributions to the visual evoked potential. *Exp. Brain Res.* 94, 183–192.
- Wahba, G., 1976. Hiosplines with knots which are order statistics. *J. R. Stat. Soc. B* 38, 140–151.

- Wahba, G., 1981. Numerical experiments with the thin plate histspline. *Comm. Statist. - Theor. Meth.* 10, 2475–2514.
- Wahba, G., 1990. Spline models for observational data. Vol. 59 of CBMS-NSF Regional Conference Series in Applied Mathematics. SIAM, Philadelphia.
- Wang, R., Perreau-Guimaraes, M., Carvalhaes, C., Suppes, P., 2012. Using phase to recognize english phonemes and their distinctive features in the brain. *Proc. Natl. Acad. Sci.* 109, 20685–20690.
- Winter, W. R., Nunez, P. L., Ding, J., Srinivasan, R., 2007. Comparison of the effect of volume conduction on EEG coherence with the effect of field spread on MEG coherence. *Stat. Med.* 26, 3946–3957.
- Wood, S. N., 2003. Thin plate regression splines. *J. R. Statist. Soc. B*, 95–114.
- Yao, 1996. The equivalent source technique and cortical imaging. *Electroencephalogr. Clin. Neurophysiol.* 98, 478–483.
- Yao, D., 2002. High-resolution EEG mapping: a radial-basis function based approach to the scalp laplacian estimate. *Clin. Neurophysiol.* 113, 956–967.
- Yao, D., Zhou, Y., Zeng, M., Fan, S., Lian, J., Wu, D., Ao, X., Chen, L., He, B., 2001. A study of equivalent source techniques for high-resolution EEG imaging. *Phys. Med. Biol.* 46, 2255–2266.
- Zhai, Y., Yao, D., 2004. A radial-basis function based surface Laplacian estimate for a realistic head model. *Brain Topogr.* 17, 55–62.